Impact loading history modulates hip fracture load and location: a finite element simulation study of the proximal femur in female athletes

Shinya Abe, Nathaniel Narra, Riku Nikander, Jari Hyttinen, Reijo Kouhia, Harri Sievänen

PII: S0021-9290(18)30416-0
DOI: https://doi.org/10.1016/j.jbiomech.2018.05.037
Reference: BM 8731

To appear in: *Journal of Biomechanics*

Received Date: 19 September 2017
Revised Date: 11 April 2018
Accepted Date: 30 May 2018

Please cite this article as: S. Abe, N. Narra, R. Nikander, J. Hyttinen, R. Kouhia, H. Sievänen, Impact loading history modulates hip fracture load and location: a finite element simulation study of the proximal femur in female athletes, *Journal of Biomechanics* (2018), doi: https://doi.org/10.1016/j.jbiomech.2018.05.037

Ms. No. BM-D-17-00970R1

Title

Impact loading history modulates hip fracture load and location: a finite element simulation study of the proximal femur in female athletes

Shinya Abe [a,*], Nathaniel Narra [b], Riku Nikander [c,d,e], Jari Hyttinen [b], Reijo Kouhia [a], Harri Sievänen [f,**]

[a]Laboratory of Civil Engineering, Tampere University of Technology, Tampere, Finland
[b]BioMediTech Institute and Faculty of Biomedical Sciences and Engineering, Tampere University of Technology, Tampere, Finland
[c]Gerontology Research Center, Faculty of Sports Sciences, University of Jyväskylä, Jyväskylä, Finland
[d]Central Hospital of Central Finland, Jyväskylä, Finland
[e]GeroCenter Foundation for Aging Research and Development, Jyväskylä, Finland
[f]The UKK Institute for Health Promotion Research, Tampere, Finland

Corresponding authors:

* Correspondence to: S. Abe, Laboratory of Civil Engineering, Tampere University of Technology, Tekniikankatu 12, FI-33720, Tampere, Finland.
Tel.: +358 40 8400364, email address: shinya.abe@tut.fi
** Correspondence to: H. Sievänen, The UKK Institute for Health Promotion Research, Kaupinpuistonkatu 1, FI-33500, Tampere, Finland.
Tel.: +358 32 829237, email address: harri.sievanen@uta.fi

Submitted as "**Original Article**"

Word count

- Abstract: 250
- Manuscript: 3990 (revised version), 3325 (initial submission)

Keywords. Bone strength, Finite element modeling, Exercise, Falling, Femoral neck

A supplemental data, describing the sensitivity analysis and it's result, is included in this submission.

Abstract

Sideways falls impose high stress on the thin superolateral cortical bone of the femoral neck, the region regarded as a fracture-prone region of the hip. Exercise training is a natural mode of mechanical loading to make bone more robust. Exercise-induced adaptation of cortical bone along the femoral neck has been previously demonstrated. However, it is unknown whether this adaption modulates hip fracture behavior. The purpose of this study was to investigate the influence of specific exercise loading history on fall-induced hip fracture behavior by estimating fracture load and location with proximal femur finite element (FE) models created from magnetic resonance images (MRI) of 111 women with distinct exercise histories: 91 athletes (aged 24.7 ± 6.1 years, >8 years competitive career) and 20 women as controls (aged 23.7 ± 3.8 years). The athletes were divided into five groups based on typical loading patterns of their sports: high-impact (H-I: 9 triple-jumpers and 10 high jumpers), odd-impact (O-I: 9 soccer and 10 squash players), high-magnitude (H-M: 17 power-lifters), repetitive-impact (R-I: 18 endurance runners), and repetitive non-impact (R-NI: 18 swimmers). Compared to the controls, the H-I, O-I, and R-I groups had significantly higher (11 to 26 %, $p < 0.05$) fracture loads. Also, the fracture location in the H-I and O-I groups was significantly more proximal (7 to 10%) compared to the controls. These results suggest that an exercise loading history of high impacts, impacts from unusual directions, or repetitive impacts increases the fracture load and may lower the risk of fall-induced hip fracture.

1. Introduction

Cortical bone at the inferomedial side of the human femoral neck is thicker than at the superolateral side because of asymmetric loading in bipedal locomotion, which imposes higher compressive and smaller tensile stress at the inferomedial and superolateral cortices, respectively (Lotz et al., 1995; Mayhew et al., 2005). With aging, the amount of vigorous physical activity (PA) decreases, and PA mainly consists of less intensive walking (Husu et al., 2016). Decreased skeletal loading may accentuate thinning of the femoral neck cortex, and it has been observed that the cortical thickness at the posterior side of the superolateral region decreases fivefold from the age of 25 years to the age of 85 years (Poole et al., 2010). This site-specific cortical thinning is likely to contribute to hip fragility (Mayhew et al., 2005).

More than 90 % of the hip fractures are caused by falls (Grisso et al., 1991; Parkkari et al., 1999; Yang et al., 2016). The superolateral cortex of the femoral neck is considered particularly vulnerable during a sideways fall, which imposes high impact force on the greater trochanter and unusually high compressive stress at the superolateral region (de Bakker et al., 2009; Verhulp et al., 2008). Peak magnitude of this fall-induced stress can be four times greater than during normal gait (Lotz et al., 1995). Consistent evidence indicates that hip fractures mostly initiate in this region (Carpenter et al., 2005; de Bakker et al., 2009).

General PA and specific exercise training are natural modes of mechanical loading of bones. Since bone structure adapts to habitual mechanical loading (Frost, 2003; Ruff et al., 2006), effective loading modes can make bone stronger. Previously, we showed that the femoral neck cortical bone in female athletes with a history of high impact loading and/or impact loading from unusual directions was thicker also in the superolateral region (Nikander et al., 2009). Moreover, finite element (FE) models created from the same proximal femur data (Abe et al., 2016) indicated that the history of not only aforementioned impact exercises but also repetitive impacts generated by endurance running were associated with lower fall-induced stress at the superolateral cortex. However, whether this apparent structural adaptation translates into a reduced hip fracture risk is not yet known, as stress

alone is not sufficient to infer the risk. Evaluating fracture loads, as suggested by numerous studies, is essential for evaluating fracture risk (Bessho et al., 2009; Dragomir-Daescu et al., 2011; Keyak et al., 1998; Koivumäki et al., 2012; Schileo et al., 2014). Therefore, the objective of the present study was to elaborate whether specific long-term exercise loading history can modulate fracture load and location that may eventually lower hip fracture risk.

2. Materials and Methods

2.1. Participants

Proximal femur magnetic resonance images (MRI) of 91 adult female athletes (aged 24.7 ± 6.1 years), competing actively at national or international level, and 20 habitually active female control participants (aged 23.7 ± 3.8 years) were obtained from our previous study (Nikander et al., 2009). According to our standard exercise classification scheme (Nikander et al., 2006, 2005), the athletes were divided into five different groups based on the typical loading patterns of their sports: high-impact (H-I) (9 triple- and 10 high-jumpers); odd-impact (O-I) (9 soccer and 10 squash players); high-magnitude (H-M) (17 power-lifters); repetitive-impact (R-I) (18 endurance runners); and the repetitive, non-impact group (R-NI) (18 swimmers). The control participants did recreational exercise 2–3 times a week, but had never taken part in any sports at the competitive level. The study protocol was approved by the Ethics Committee of the Pirkanmaa Hospital District, and written informed consent was obtained from each participant.

Body height and weight (BW) of the participants were measured in light indoor clothing without shoes with standard methods. Questionnaires were completed by all participants in order to obtain their training history including weekly sport-specific training hours and the number of training sessions during at least the five preceding years (Nikander et al., 2009).

2.2. MRI scanning procedure

Participants' hip regions were scanned using a 1.5-T MRI system (Avanto Syngo MR B15, Siemens, Erlangen, Germany). The imaging sequence was a standardized axial T1-weighted gradient

echo volumetric interpolated breath-hold (VIBE)-examination with the following parameters: FOV 35×26 cm, TR 15.3 ms, TE 3.32 ms, slice thickness 1 mm without gaps, echo train length = 1, flip angle =10°, matrix 384×288, the in-plane resolution (pixel size) 0.9 mm×0.9 mm. Sagittal, axial, and coronal images of the hip region of the dominant side were scanned with two half-Fourier acquisition single-shot turbo spin-echo localization series. The scanned body volume covered the proximal femur from the top of the femoral head to the subtrochanteric level of the femoral diaphysis. The reconstructed imaging plane was adjusted so that the cross-sectional plane of the femoral neck was perpendicular to the femoral neck axis (Nikander et al., 2009).

2.3. FE model construction

The proximal femur FE models from the MRI data of all 111 participants were created previously (Abe et al., 2016). In short, the MRI data were first manually segmented by delineating the periosteal and endocortical boundaries of cortical bone along the proximal femur with in vivo precision of about 1% (Sievänen et al., 2007b). Then, the obtained femur geometries were converted into a volume mesh and its surface was smoothed using a method by Taubin (1995) prior to the generation of 3D solid bodies in SolidWorks (SolidWorks Corp., Waltham, MA, USA). The resulting proximal femur geometry consisted of individually segmented cortical and trabecular bone volumes, the latter denoting the volume within the endocortical bone boundary. Trabecular bone is a nonhomogeneous porous structure, but in this study, it was modeled as a non-porous homogeneous material because pertinent information could not be obtained from the present MRI data. Therefore, the present study exclusively assessed the influence of the cortical geometry on the hip fracture behavior, whereas the potential influence of inhomogeneous trabecular bone distribution was not addressed. The individual 3D solid body geometries of the proximal femur were then imported into ANSYS (ANSYS Inc., Houston, PA, USA) for the FE meshing and analysis.

To simulate a sideways fall, the femoral shaft was tilted at 10° with respect to the ground and the femoral neck was internally rotated by 15° (Fig. 1) (Courtney et al., 1994). Similar boundary conditions (BC) used in previous studies (Helgason et al., 2014; Schileo et al., 2014) were adopted in

the present models (Fig. 1). The loading force and restraining BCs were applied through the femoral head- and trochanter-protecting PMMA caps, and an aluminum distal pot. The force was applied to the femoral head through the cap at a defined angle. The trochanter PMMA cap was restrained in the direction of the force while a hinge-type restraining BC was applied to the distal side of the aluminum pot. A 10-noded tetrahedral finite element was used to mesh all components. For the entire proximal femur, the PMMA caps, and the boundary between the distal end of the modeled proximal femur bone and the distal pot, 1 mm element size was used while 4 mm element size was set for the rest of the distal pot. On average, each bone model comprised approximately 1,600,000 elements and 2,300,000 nodes. The bone tissue was modeled as a homogeneous isotropic, linear elastic material, cortical and trabecular bone separately. Young's moduli (E) of 17 GPa (Duda et al., 1998; Lengsfeld et al., 1996; Polgár et al., 2003), 1500 MPa (Duda et al., 1998; Polgár et al., 2003), 70 GPa (Schileo et al., 2014), and 2 GPa (Schileo et al., 2014) were applied for the cortical bone, trabecular bone, the aluminum distal pot, and the protecting PMMA caps, respectively. Poisson's ratio was assumed as 0.33 for all materials (Duda et al., 1998; Lengsfeld et al., 1996; Polgár et al., 2003).

2.4. Fracture load

For estimating the fracture load of each proximal femur, a simple maximum principal strain criterion (Schileo et al., 2014, 2008b) was adopted. First, surface nodal strains of the whole proximal femur and their nodal coordinates were obtained from the FE models. Each nodal strain was averaged with its neighboring nodal strains within a circle of 3 mm radius to remove local effects and to ensure the hypothesis of continuum media (Schileo et al., 2014; Verhulp et al., 2008). Then, principal strains were calculated for each node from the average nodal strain tensor. The fracture load was defined as the load when either one nodal maximum principal strain was greater than tensile yield limit (0.73%) or the absolute value of the minimum principal strain was greater than compressive yield limit (1.04%) (Bayraktar et al., 2004). Using the linearity of the model, the magnitude of load was increased until one nodal principal strain value exceeded the elastic limit. In addition, the fracture mode (by tension or compression) was also determined for each femur. Due to the use of linear FE

models, the predicted fracture load in this study denotes the load at the onset of fracture similar to the previous studies (Nishiyama et al., 2013; Schileo et al., 2014; Verhulp et al., 2008).

2.5. Fracture location

Surface nodal coordinates obtained from the fracture load estimation were utilized to determine the fracture location. The fracture location was determined in two ways: 1) as a *polar angle* (in º) and 2) as a *relative axial location* (in %) (Fig. 2). The polar angle was defined as how far the fracture node was, in clockwise direction, from the most superior point (0º) of the femoral neck cross-section (Fig. 2 B). Furthermore, this *polar angular location* was presented as octant-wise categories within 45º octant regions each representing the following anatomic segments of the given femoral neck cross-section: superior (S), superoposterior (SP), posterior (P), inferoposterior (IP), inferior (I), inferoanterior (IA), anterior (A), and superoanterior (SA) octants (Fig. 2 C).

The *relative axial location* was defined as the relative location (in %) from the most proximal cross-section of the femoral neck along its axis to the distal cross-section where femoral neck meets the greater trochanter (Fig. 2 D). The *relative axial location* was also categorized into either 1) cervical fracture if the fracture location was between the proximal (0%) and the distal (100%) cross-sections otherwise it was categorized as 2) trochanteric fracture (>100%). Furthermore, the cervical fracture was divided into three equally long macro-regions: subcapital (between 0 % and 33.3 %), transcervical (between 33.4 % and 66.6 %) and basicervical (between 66.7 % and 100%) regions similarly to the previous study (Schileo et al., 2014) (Fig. 2 D). MATLAB (MathWorks, Inc., Natick, MA, USA) was used to estimate the fracture load and location.

2.6. Statistical Analysis

Statistical analyses were performed with SPSS 24.0 (IBM Corp., Armonk, NY, USA). Mean and SD of fracture load and locations were given as descriptive statistics. Differences in fracture load between each exercise group and the control group was estimated by analysis of variance (ANOVA) and analysis of covariance (ANCOVA) using body weight as a covariate. Logarithmic transformations of the fracture load was performed prior to both ANOVA and ANCOVA to control

for the skewness of the data. Percentage differences of the fracture load between each exercise loading group and control group were calculated by taking anti-log of unadjusted and BW-adjusted mean fracture loads. Since fracture locations (the *polar angular* and *relative axial locations*) were not normally distributed, between-group differences were estimated by non-parametric Mann-Whitney U test. Exercise groups were not compared to each other. A p value of less than 0.05 was considered statistically significant.

3. Results

3.1. Descriptive data of participants

Age, body height, BW, sport-specific training hours/week, training sessions/week, and duration of competitive career of loading groups are shown in Table 1. Compared with control participants, athletes had more training hours and training sessions per week, besides their long history of competing career. Also, majority of athletes in the present study started their sport-specific training in adolescence or early adulthood (Table 1).

3.2. Fracture load

Table 2 shows unadjusted mean (SD) of the fracture load, and unadjusted and BW-adjusted mean percentage differences (95% CI) in the fracture loads between each exercise group and the control group. Fracture loads ranged from 2.1 kN to 4.4 kN. Fracture loads in the H-I, O-I, and R-I groups were significantly ($p < 0.05$) higher compared to the control group. Unadjusted mean differences of H-I, O-I, and R-I compared with the control group were 15%, 12%, and 14% respectively. Similarly, BW-adjusted mean differences of H-I, O-I, and R-I were 14%, 11%, and 26% respectively. Compression was the failure mode in all 111 cases.

3.3. Fracture location

Table 3 shows means (SD), and ranges of the *polar angular* and the *relative axial fracture locations.* Table 4 shows their anatomical regional locations. Fracture locations were also mapped in each group (Fig. 3). In general, the mean *polar angular location* among the loading groups ranged

from 30 to 41° (Table 3). This angular span was in the superoposterior octant where the majority of simulated fractures (75 out of 111, 68%) were located (Table 4). There was no significant difference in the *polar angular location* observed between any of exercise and the control group. The mean *relative axial location* ranged from 87 to 98% (Table 3) corresponding to basicervical region (Table 4). Majority of simulated fractures (90 out of 111, 81%) were located in this region (Table 4). The *relative axial locations* in the H-I and O-I were significantly ($p < 0.05$) different (7% and 10% more proximal respectively) compared to the control group.

4. Discussion

Fracture loads and locations at the proximal femur were estimated in this study using proximal femur FE models of 111 young adult women to evaluate whether the specific long-term exercise history modulated the fall-induced fracture behavior. In general, the magnitudes of observed fracture loads (2.1 kN to 4.4 kN) were within the range reported by Schileo et al. (2014). The present results also showed that the fracture initiated mostly at the superolateral region of the femoral neck, especially at the superoposterior octant of the basicervical region (Table 4 and Fig. 3). This was in close agreement with previous experimental and modeling studies (Carpenter et al., 2005; de Bakker et al., 2009; Dragomir-Daescu et al., 2011; Lotz et al., 1995; Nawathe et al., 2015; Schileo et al., 2014; Verhulp et al., 2008). A particularly important finding in the present study was that the mean fracture loads in the H-I, O-I, and R-I groups were significantly higher (11 to 26%) compared to the control group. This indicates that exercise loading history comprising high vertical impacts, impacts from unusual directions, or a great number of repetitive impacts during adolescence and early adulthood may contribute to the reduced hip fracture risk.

The present observations in the H-I, O-I, and R-I groups are most likely attributed to the exercise-induced adaptation of the femoral neck cortical bone: through regional cortical thickening in the H-I and O-I groups, and different femoral neck geometry in the R-I group. Regional cortical thickening was evident at the inferior, anterior, and posterior quadrants of the femoral neck in the H-I group; and at the anterior, posterior, and superior quadrants in the O-I group (Nikander et al., 2009). In contrast,

such a regional cortical thickening was not found in the R-I group (Nikander et al, 2009) whereas the geometric shape of the femoral neck cross-section was more circular in this group (Narra et al., 2013). A round shape of the femoral neck cross-section is an important geometric factor contributing to its strength (Bryan et al., 2009). Compared to an oval-shaped bone, a circular bone is mechanically more robust regardless of the loading direction. Moreover, a circular femoral neck cross-section, typically observed among physically more active medieval people, were estimated to experience 1.3-1.5 times less fall-induced stress compared to a more oval-shaped cross-section typical in present-day, habitually more sedentary people (Sievänen et al., 2007a). The BW-adjusted 26% benefit in fracture load observed in the present R-I group is fully consistent with this estimation.

Another notable finding was that the *relative axial fracture locations* in the H-I and O-I groups were slightly but significantly more proximal (along the neck axis) compared to the control group while the R-I group did not differ from the controls. This shift may be due to the regionally thicker cortical bone in the typical fracture-prone region which may transfer the peak bending stresses towards the narrower femoral neck (mid neck). This further indicates that higher fracture load results in the H-I and O-I groups might be due to the regional cortical thickening while the finding in the R-I group was due to the more circular femoral neck cross-section.

Based on the bone remodeling theory (Huiskes et al., 1987), new bone formation occurs when the loading induced strain energy exceeds certain homeostatic values by 75% (Kerner et al., 1999). The distribution of strain energy on the femoral neck during 15 different exercise types (long jump, vertical jump, walking, stair walking, squat with and without weight, and more) have been evaluated using both FE and musculoskeletal modeling (Kłodowski et al., 2011; Martelli et al., 2014). Martelli and colleagues (2014) reported that the H-I exercise (one-legged long jump) caused substantially high strain energy at femoral neck exceeding homeostatic value by about 500%. Elaborating the loading characteristics of the five distinct exercise types assessed in this study may explain why no beneficial results were observed in the H-M and R-NI groups despite high loading magnitudes or volume of training. Combination of moderate-to-high peak reaction forces and high rate of loading rate due to the ground impacts seems essential for the beneficial structural adaptation of the femoral neck cortical

bone. The peak reaction forces and the estimated impact rates (BW s^{-1}) are 12–20 times BW and 400–480 BW s^{-1} in the H-I loading (Heinonen et al., 2001; Ramey and Williams, 1985), and 2–3.5 times BW and 20–180 BW s^{-1} in the O-I and R-I loading (Ball, 2013; Dayakidis and Boudolos, 2006; Kluitenberg et al., 2012; Logan et al., 2010; Munro et al., 1987; Smith et al., 2004). In swimming, some impact loading may occur at the push-off phase of turning, but the peak reaction force and loading rate are considerably smaller (< 1.5 times BW, and <10 BW s^{-1} respectively) (Blanksby et al., 1996; Lyttle et al., 1999). While the peak reaction forces in the H-M are comparable (2–3 times BW) to the O-I and R-I exercises, the loading rate remains essentially smaller (5–6 BW s^{-1}) (Swinton et al., 2012). Altogether, moderate-to-high reaction force alone seems inadequate but it needs to be delivered at high loading rate to attain beneficial structural adaption within the femoral neck cortical bone.

There are limitations in the present study. First, the pixel size (0.9 mm) of the original MRI data was almost twice larger compared to previous QCT-based FE modeling studies (Bessho et al., 2009; Dragomir-Daescu et al., 2011; Koivumäki et al., 2012; Nishiyama et al., 2013; Schileo et al., 2014). However, while the QCT provides higher resolution and data on bone apparent density (proxy of material property), MRI has been found adequately valid for cortical geometry (Gomberg et al., 2005; Sievänen et al., 2007b). Besides, exposing fertile young adult women to ionizing radiation from QCT for non-diagnostic purposes would have been ethically unacceptable.

Second, due to inability to measure bone apparent density data with MRI, it was not possible to assign inhomogeneous material properties in the present study. It is known that the proximal femur is almost completely filled with porous structure of the trabecular bone, which is usually modeled as an inhomogeneous density-based material in the FE model. Obviously, the use of inhomogeneous material properties for the trabecular bone may have enhanced the model accuracy to some extent. However, it has been found previously that a homogeneous FE-model resulted in only marginally less accurate stress predictions compared to the actual experimental stress than the inhomogeneous model (R^2 = 0.89 and 0.91 respectively) (Taddei et al., 2006). Also, Koivumäki et al. (2010) reported 85% agreement between the homogeneous models with the experimental fracture location. On the other

hand, the comparison by Taddei et al. (2006) was based only on a single femur model and in the physiological conditions including walking and single leg stance, but not in the sideways falling situation. Thus, this calls for further investigation on the validity of applying homogeneous material properties in the sideways falling situation with a larger sample size. Because we employed fixed Young's moduli for cortical (17GPa) and trabecular (1500 MPa) bone compartments and treated them as the homogeneous material, the present study was limited to evaluate only the influence of the cortical geometry on the fracture load during a fall. The sensitivity of our models to the variation of cortical and trabecular E values were also evaluated in the present study (Details of this sensitivity analysis and results are available in the Supplementary material). According to this sensitivity analysis, the error in between-group differences of unadjusted mean fracture load induced by the substantial variation of cortical and trabecular moduli was within 3%, which was clearly smaller than observed in the H-I, O-I and R-I groups (11 % to 14%, Table 2). Therefore, our choice to employ homogeneous material properties can be considered adequate in terms of evaluating the influence of the cortical geometry on fracture load.

Third, the present FE models created from proximal femur MRI were not validated against mechanical testing unlike previous QCT-based FE modeling studies of cadaver bones (Bessho et al., 2009; Koivumäki et al., 2012; Schileo et al., 2014). Due to these aforementioned limitations, and to comply with validated QCT-based proximal femur FE modeling studies, we adopted similar BCs and loading conditions (Helgason et al., 2014; Schileo et al., 2014). Importantly, despite the MRI-related limitations, the range of fracture loads in the present study was completely in line with the previously reported values of QCT-based FEM study (Schileo et al., 2014). However, proximal femora in their study were obtained from older people aged from 62 to 84 years, which casts some doubt on the fracture load range found in the present young physically active population where higher fracture loads could have been expected. Nicks et al. (Nicks et al., 2013) reported the femoral neck trabecular volumetric bone mineral density (vBMD) from 20-29 years old female was 0.268 g/cm^3. By converting this vBMD value to the Young's modulus using equations found in literature (Morgan et al., 2003; Schileo et al., 2014, 2008a), a Young's modulus of about 2600 MPa is yielded, which is

much higher than 1500 MPa used in the present study. Thus, the present fracture load values in the young athletic population was likely underestimated. It was shown that the mean fracture load was increased by approximately 15% by changing the trabecular E value from 1500 MPa to 3000 MPa (Fig. A1 in Supplementary material). The effect of the variation of cortical and trabecular E values on the magnitude of fracture load was also evaluated in the sensitivity analysis (Details are available in Supplementary material). However, it is noted that the main focus of the present study was to evaluate the relative fracture load of the proximal femur between each exercise group and the control group. Considering the apparent fact that the athletic groups have higher bone density at the proximal femur than their nonathletic peers (Nikander et al, 2009), it is likely that between-group difference in fracture load could have been higher.

In conclusion, the present simulation study based on a large sample study of the proximal femora indicates that long-term exercise loading history of high vertical impacts, impacts from unusual directions, or a great number of repetitive impacts led to higher fracture load and altered fracture location, which may translate into lower risk to sustain a hip fracture as a result of a fall. As a clinical prospect, it can be speculated that the impact exercises provide natural mechanical loading to femoral neck for increasing or maintaining its strength against fall-induced impacts.

Conflict of interest statement

All authors state that they have no conflicts of interest.

Acknowledgements

The authors thank all study participants. This work was funded by Tampere University of Technology's (TUT) Graduate School; the Doctoral Education Council of Computing and Electrical Engineering of TUT; and Human Spare Parts project from the Finnish Funding Agency for Technology and Innovation (TEKES).

References

Abe, S., Narra, N., Nikander, R., Hyttinen, J., Kouhia, R., Sievänen, H., 2016. Exercise loading history and femoral neck strength in a sideways fall: A three-dimensional finite element modeling study. Bone 92, 9–17. doi:10.1016/j.bone.2016.07.021

Ball, K., 2013. Loading and performance of the support leg in kicking. J. Sci. Med. Sport 16, 455–459. doi:10.1016/j.jsams.2012.10.008

Bayraktar, H.H., Morgan, E.F., Niebur, G.L., Morris, G.E., Wong, E.K., Keaveny, T.M., 2004. Comparison of the elastic and yield properties of human femoral trabecular and cortical bone tissue. J. Biomech. 37, 27–35. doi:10.1016/S0021-9290(03)00257-4

Bessho, M., Ohnishi, I., Matsumoto, T., Ohashi, S., Matsuyama, J., Tobita, K., Kaneko, M., Nakamura, K., 2009. Prediction of proximal femur strength using a CT-based nonlinear finite element method: Differences in predicted fracture load and site with changing load and boundary conditions. Bone 45, 226–231. doi:10.1016/j.bone.2009.04.241

Blanksby, B.A., Gathercole, D.G., Marshall, R.N., 1996. Force plate and video analysis of the tumble turn by age-group swimmers. J. Swim. Res. 11, 40–45.

Bryan, R., Nair, P.B., Taylor, M., 2009. Use of a statistical model of the whole femur in a large scale, multi-model study of femoral neck fracture risk. J. Biomech. 42, 2171–2176. doi:10.1016/j.jbiomech.2009.05.038

Carpenter, R.D., Beaupré, G.S., Lang, T.F., Orwoll, E.S., Carter, D.R., 2005. New QCT analysis approach shows the importance of fall orientation on femoral neck strength. J. Bone Miner. Res. 20, 1533–1542. doi:10.1359/JBMR.050510

Courtney, A.C., Wachtel, E.F., Myers, E.R., Hayes, W.C., 1994. Effects of loading rate on strength of the proximal femur. Calcif. Tissue Int. 55, 53–58. doi:10.1007/BF00310169

Dayakidis, M.K., Boudolos, K., 2006. Ground reaction force data in functional ankle instability

during two cutting movements. Clin. Biomech. 21, 405–411. doi:10.1016/j.clinbiomech.2005.11.010

de Bakker, P.M., Manske, S.L., Ebacher, V., Oxland, T.R., Cripton, P.A., Guy, P., 2009. During sideways falls proximal femur fractures initiate in the superolateral cortex: Evidence from high-speed video of simulated fractures. J. Biomech. 42, 1917–1925. doi:10.1016/j.jbiomech.2009.05.001

Dragomir-Daescu, D., Op Den Buijs, J., McEligot, S., Dai, Y., Entwistle, R.C., Salas, C., Melton, L.J., Bennet, K.E., Khosla, S., Amin, S., 2011. Robust QCT/FEA models of proximal femur stiffness and fracture load during a sideways fall on the hip. Ann. Biomed. Eng. 39, 742–755. doi:10.1007/s10439-010-0196-y

Duda, G.N., Heller, M., Albinger, J., Schulz, O., Schneider, E., Claes, L., 1998. Influence of muscle forces on femoral strain distribution. J. Biomech. 31, 841–846. doi:10.1016/S0021-9290(98)00080-3

Frost, H.M., 2003. Bone's mechanostat: A 2003 update. Anat. Rec. A. Discov. Mol. Cell Evol. Biol. 275, 1081–1101. doi:10.1002/ar.a.10119

Gomberg, B.R., Saha, P.K., Wehrli, F.W., 2005. Method for cortical bone structural analysis from magnetic resonance images. Acad. Radiol. 12, 1320–1332. doi:10.1016/j.acra.2005.06.012

Grisso, J.A., Kelsey, J.L., Strom, B.L., Chiu, G.Y., Maislin, G., O'Brien, L.A., Hoffman, S., Kaplan, F., 1991. Risk factors for falls as a cause of hip fracture in women. The Northeast Hip Fracture Study Group. N. Engl. J. Med. 324, 1326–1331. doi:10.1056/NEJM199105093241905

Heinonen, A., Sievänen, H., Kyröläinen, H., Perttunen, J., Kannus, P., 2001. Mineral mass, size, and estimated mechanical strength of triple jumpers' lower limb. Bone 29, 279–285. doi:10.1016/S8756-3282(01)00574-9

Helgason, B., Gilchrist, S., Ariza, O., Chak, J.D., Zheng, G., Widmer, R.P., Ferguson, S.J., Guy, P.,

Cripton, P.A., 2014. Development of a balanced experimental-computational approach to understanding the mechanics of proximal femur fractures. Med. Eng. Phys. 36, 793–799. doi:10.1016/j.medengphy.2014.02.019

Huiskes, R., Weinans, H., Grootenboer, H.J., Dalstra, M., Fudala, B., Slooff, T.J., 1987. Adaptive bone-remodeling theory applied to prosthetic-design analysis. J. Biomech. 20, 1135–1150. doi:10.1016/0021-9290(87)90030-3

Husu, P., Suni, J., Vähä-Ypyä, H., Sievänen, H., Tokola, K., Valkeinen, H., Mäki-Opas, T., Vasankari, T., 2016. Objectively measured sedentary behavior and physical activity in a sample of Finnish adults: a cross-sectional study. BMC Public Health 16, 920. doi:10.1186/s12889-016-3591-y

Kerner, J., Huiskes, R., van Lenthe, G.H., Weinans, H., van Rietbergen, B., Engh, C.A., Amis, A.A., 1999. Correlation between pre-operative periprosthetic bone density and post-operative bone loss in THA can be explained by strain-adaptive remodelling. J. Biomech. 32, 695–703. doi:10.1016/S0021-9290(99)00041-X

Keyak, J.H., Rossi, S.A., Jones, K.A., Skinner, H.B., 1998. Prediction of femoral fracture load using automated finite element modeling. J. Biomech. 31, 125–133. doi:10.1016/S0021-9290(97)00123-1

Kłodowski, A., Rantalainen, T., Mikkola, A., Heinonen, A., Sievänen, H., 2011. Flexible multibody approach in forward dynamic simulation of locomotive strains in human skeleton with flexible lower body bones. Multibody Syst. Dyn. 25, 395–409. doi:10.1007/s11044-010-9240-9

Kluitenberg, B., Bredeweg, S.W., Zijlstra, S., Zijlstra, W., Buist, I., 2012. Comparison of vertical ground reaction forces during overground and treadmill running. A validation study. BMC Musculoskelet. Disord. 13, 235. doi:10.1186/1471-2474-13-235

Koivumäki, J.E.M., Thevenot, J., Pulkkinen, P., Kuhn, V., Link, T.M., Eckstein, F., Jämsä, T., 2012. Ct-based finite element models can be used to estimate experimentally measured failure loads in the proximal femur. Bone 50, 824–829. doi:10.1016/j.bone.2012.01.012

Koivumäki, J.E.M., Thevenot, J., Pulkkinen, P., Salmi, J.A., Kuhn, V., Lochmüller, E.M., Link, T.M., Eckstein, F., Jämsä, T., 2010. Does femoral strain distribution coincide with the occurrence of cervical versus trochanteric hip fractures? An experimental finite element study. Med. Biol. Eng. Comput. 48, 711–717. doi:10.1007/s11517-010-0622-1

Lengsfeld, M., Kaminsky, J., Merz, B., Franke, R.P., 1996. Sensitivity of femoral strain pattern analyses to resultant and muscle forces at the hip joint. Med. Eng. Phys. 18, 70–78. doi:10.1016/1350-4533(95)00033-X

Logan, S., Hunter, I., Hopkins, J.T., Feland, J.B., Parcell, A.C., 2010. Ground reaction force differences between running shoes, racing flats, and distance spikes in runners. J. Sport. Sci. Med. 9, 147–153. doi:10.1055/s-0033-1338501

Lotz, J.C., Cheal, E.J., Hayes, W.C., 1995. Stress distributions within the proximal femur during gait and falls: Implications for osteoporotic fracture. Osteoporos. Int. 5, 252–261. doi:10.1007/BF01774015

Lyttle, A.D., Blanksby, B.A., Elliott, B.C., Lloyd, D.G., 1999. Investigating kinetics in the freestyle flip turn push-off. J. Appl. Biomech. 15, 242–252.

Martelli, S., Kersh, M.E., Schache, A.G., Pandy, M.G., 2014. Strain energy in the femoral neck during exercise. J. Biomech. 47, 1784–1791. doi:10.1016/j.jbiomech.2014.03.036

Mayhew, P.M., Thomas, C.D., Clement, J.G., Loveridge, N., Beck, T.J., Bonfield, W., Burgoyne, C.J., Reeve, J., 2005. Relation between age, femoral neck cortical stability, and hip fracture risk. Lancet 366, 129–135. doi:10.1016/S0140-6736(05)66870-5

Morgan, E.F., Bayraktar, H.H., Keaveny, T.M., 2003. Trabecular bone modulus-density relationships depend on anatomic site. J. Biomech. 36, 897–904. doi:10.1016/S0021-9290(03)00071-X

Munro, C.F., Miller, D.I., Fuglevand, A.J., 1987. Ground reaction forces in running: A reexamination. J. Biomech. 20, 147–155. doi:10.1016/0021-9290(87)90306-X

Narra, N., Nikander, R., Viik, J., Hyttinen, J., Sievänen, H., 2013. Femoral neck cross-sectional geometry and exercise loading. Clin. Physiol. Funct. Imaging 33, 258–266. doi:10.1111/cpf.12022

Nawathe, S., Nguyen, B.P., Barzanian, N., Akhlaghpour, H., Bouxsein, M.L., Keaveny, T.M., 2015. Cortical and trabecular load sharing in the human femoral neck. J. Biomech. 48, 816–822. doi:10.1016/j.jbiomech.2014.12.022

Nicks, K.M., Amin, S., Melton, L.J., Atkinson, E.J., McCready, L.K., Riggs, B.L., Engelke, K., Khosla, S., 2013. Three-dimensional structural analysis of the proximal femur in an age-stratified sample of women. Bone 55, 179–188. doi:10.1016/J.BONE.2013.02.009

Nikander, R., Kannus, P., Dastidar, P., Hannula, M., Harrison, L., Cervinka, T., Narra, N.G., Aktour, R., Arola, T., Eskola, H., Soimakallio, S., Heinonen, A., Hyttinen, J., Sievänen, H., 2009. Targeted exercises against hip fragility. Osteoporos. Int. 20, 1321–1328. doi:10.1007/s00198-008-0785-x

Nikander, R., Sievänen, H., Heinonen, A., Kannus, P., 2005. Femoral neck structure in adult female athletes subjected to different loading modalities. J. Bone Miner. Res. 20, 520–528. doi:10.1359/JBMR.041119

Nikander, R., Sievänen, H., Uusi-Rasi, K., Heinonen, A., Kannus, P., 2006. Loading modalities and bone structures at nonweight-bearing upper extremity and weight-bearing lower extremity: A pQCT study of adult female athletes. Bone 39, 886–894. doi:10.1016/j.bone.2006.04.005

Nishiyama, K.K., Gilchrist, S., Guy, P., Cripton, P., Boyd, S.K., 2013. Proximal femur bone strength estimated by a computationally fast finite element analysis in a sideways fall configuration. J. Biomech. 46, 1231–1236. doi:10.1016/j.jbiomech.2013.02.025

Parkkari, J., Kannus, P., Palvanen, M., Natri, A., Vainio, J., Aho, H., Vuori, I., Järvinen, M., 1999. Majority of hip fractures occur as a result of a fall and impact on the greater trochanter of the femur: A prospective controlled hip fracture study with 206 consecutive patients. Calcif. Tissue

Int. 65, 183–187. doi:10.1007/s002239900679

Polgár, K., Gill, H.S., Viceconti, M., Murray, D.W., O'Connor, J.J., 2003. Strain distribution within the human femur due to physiological and simplified loading: finite element analysis using the muscle standardized femur model. Proc. Inst. Mech. Eng. H. 217, 173–189.

Poole, K.E., Mayhew, P.M., Rose, C.M., Brown, J.K., Bearcroft, P.J., Loveridge, N., Reeve, J., 2010. Changing structure of the femoral neck across the adult female lifespan. J. Bone Miner. Res. 25, 482–491. doi:10.1359/jbmr.090734

Ramey, M.R., Williams, K.R., 1985. Ground Reaction Forces in the Triple Jump. Int. J. Sport. Biomech. 1, 233–239.

Ruff, C., Holt, B., Trinkaus, E., 2006. Who's afraid of the big bad Wolff?: "Wolff's law" and bone functional adaptation. Am. J. Phys. Anthropol. 129, 484–498. doi:10.1002/ajpa.20371

Schileo, E., Balistreri, L., Grassi, L., Cristofolini, L., Taddei, F., 2014. To what extent can linear finite element models of human femora predict failure under stance and fall loading configurations? J. Biomech. 47, 3531–3538. doi:10.1016/j.jbiomech.2014.08.024

Schileo, E., Dall'Ara, E., Taddei, F., Malandrino, A., Schotkamp, T., Baleani, M., Viceconti, M., 2008a. An accurate estimation of bone density improves the accuracy of subject-specific finite element models. J. Biomech. 41, 2483–2491. doi:10.1016/j.jbiomech.2008.05.017

Schileo, E., Taddei, F., Cristofolini, L., Viceconti, M., 2008b. Subject-specific finite element models implementing a maximum principal strain criterion are able to estimate failure risk and fracture location on human femurs tested in vitro. J. Biomech. 41, 356–367. doi:10.1016/j.jbiomech.2007.09.009

Sievänen, H., Józsa, L., Pap, I., Järvinen, M., Järvinen, T.A., Kannus, P., Järvinen, T.L., 2007a. Fragile external phenotype of modern human proximal femur in comparison with medieval bone. J. bone Miner. Res. 22, 537–543. doi:10.1359/jbmr.070102

Sievänen, H., Karstila, T., Apuli, P., Kannus, P., 2007b. Magnetic resonance imaging of the femoral neck cortex. Acta radiol. 48, 308–314. doi:10.1080/02841850601182147

Smith, N., Dyson, R., Janaway, L., 2004. Ground reaction force measures when running in soccer boots and soccer training shoes on a natural turf surface. Sport. Eng. 7, 159–167. doi:10.1007/BF02844054

Swinton, P.A., Lloyd, R., Keogh, J.W., Agouris, I., Stewart, A.D., 2012. A biomechanical comparison of the traditional squat, powerlifting squat, and box squat. J. Strength Cond. Res. 26, 1805–1816. doi:10.1519/JSC.0b013e3182577067

Taddei, F., Cristofolini, L., Martelli, S., Gill, H.S., Viceconti, M., 2006. Subject-specific finite element models of long bones: An in vitro evaluation of the overall accuracy. J. Biomech. 39, 2457–2467. doi:10.1016/j.jbiomech.2005.07.018

Taubin, G., 1995. Curve and surface smoothing without shrinkage. Proc. IEEE Int. Conf. Comput. Vis. 852–857. doi:10.1109/ICCV.1995.466848

Verhulp, E., van Rietbergen, B., Huiskes, R., 2008. Load distribution in the healthy and osteoporotic human proximal femur during a fall to the side. Bone 42, 30–35. doi:10.1016/j.bone.2007.08.039

Yang, Y., Mackey, D.C., Liu-Ambrose, T., Feldman, F., Robinovitch, S.N., 2016. Risk factors for hip impact during real-life falls captured on video in long-term care. Osteoporos. Int. 27, 537–547. doi:10.1007/s00198-015-3268-x

Fig. 1. Loading/falling angles (A & B) and boundary conditions of the FE model (C). The femoral shaft was tilted at 10° with respect to the ground (A) and the femoral neck was internally rotated by 15° (B). Force was applied to the whole upper face of the head-protecting PMMA cap, at a described angle, while the trochanter PMMA cap was restrained in the direction of the force (Schileo et al., 2014). A 200 mm long aluminum pot was placed at 15–20 mm below the most projected part of the lesser trochanter of each proximal femur. A hinge-type restraining BC was applied to the distal side of the aluminum pot. This allowed nodes at the hinge-axis to freely rotate in the quasi-frontal plane, while all other degrees of freedom were constrained (C). This figure was adopted from Abe et al. (2016).

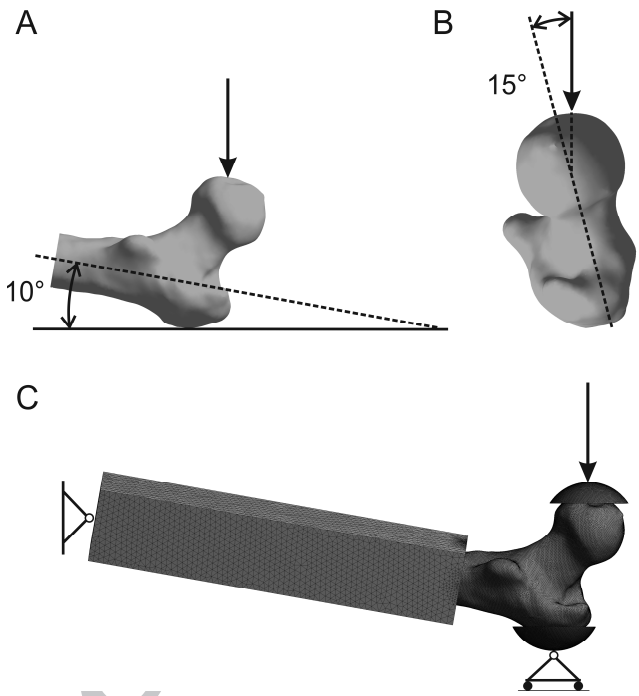

Fig. 2. Fracture location in the *polar angle* and in the *relative axial location,* and their categorizations. A) An example of the fracture node (*) which principal strain value exceeds the elastic yield limit. B) This describes the fracture location in the *polar angle* on the cross-section of the femoral neck. C) This shows the division of the femoral neck cross-section into equal 45º octant regions. The example (40° in B) corresponds to SP octant in C. D) This shows the *relative axial fracture location* and their categorization. The *relative axial location* was defined as the relative location (in %) to the femoral neck region defined by the proximal and distal planes perpendicular to the femoral neck axis. The proximal plane was defined as the plane at which the rate of change in cross-sectional area at junction from femoral head to femoral neck was the greatest while the distal plane was defined at which superior side of the femoral neck merges with the greater trochanter above the trochanteric fossa shown as a dashed-line ellipse in (D).

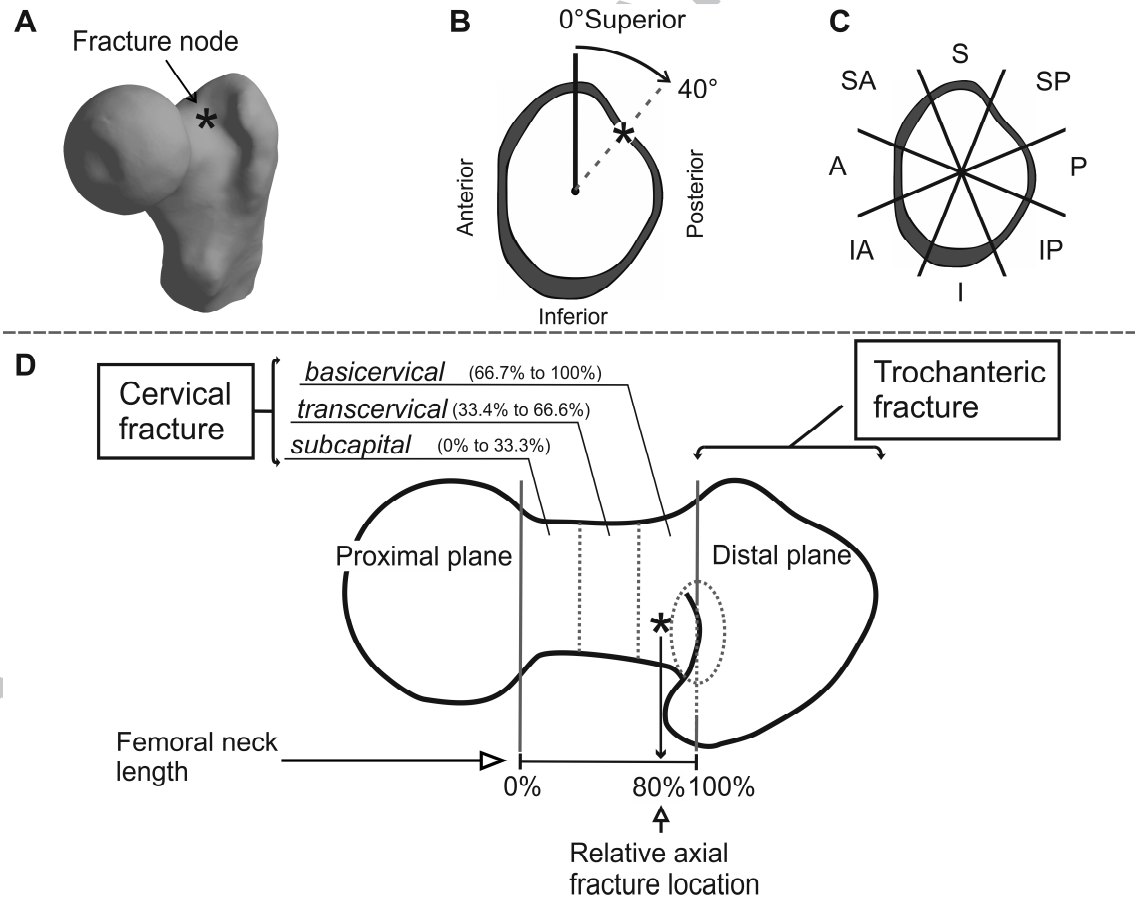

Fig. 3. Fracture location map. A) This describes corresponding regions in the octants and in the axial location either cervical (subcapital, transcervical, and basicervical) and trochanteric region. B) All 111 proximal femurs' fracture locations were mapped with *s. Different colors indicate proportion of the number of fracture in a region to the total number of fractures. C, D, E, F, G, and H are mapped fracture locations in H-I, O-I, H-M, R-I, R-NI, and control groups, respectively.

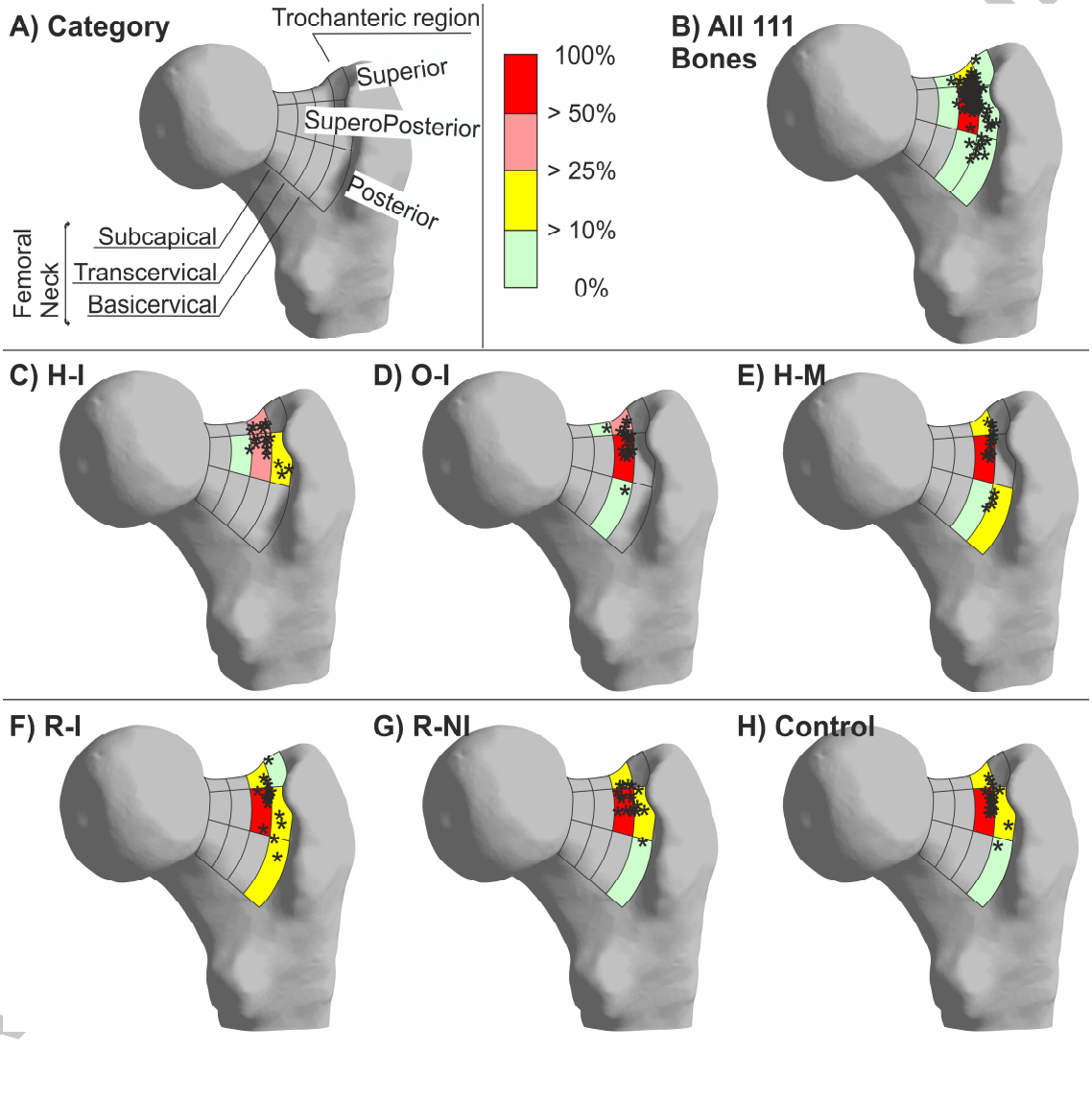

Tables

Table 1. Descriptive group characteristics (mean (SD))

Group	N	Age (years)	Height (cm)	Weight (kg)	Sport-specific training hours / week	Training sessions / week	Competing career (years)
H-I	19	22.3 (4.1)	174 (6)	60.2 (5.4)	11.5 (2.3)	6.7 (1.4)	10.1 (3.4)
O-I	19	25.3 (6.7)	165 (8)	60.8 (8.3)	9.3 (2.7)	5.7 (1.4)	9.6 (4.8)
H-M	17	27.5 (6.3)	158 (3)	63.3 (13.2)	9.1 (2.7)	5.8 (2.0)	8.0 (4.7)
R-I	18	28.9 (5.6)	168 (5)	53.7 (3.4)	10.9 (3.4)	8.7 (2.1)	12.4 (6.7)
R-NI	18	19.7 (2.4)	173 (5)	65.1 (5.6)	19.9 (4.5)	11.4 (2.0)	9.1 (2.6)
Control	20	23.7 (3.8)	164 (5)	60.0 (7.4)	2.8 (0.9)	2.8 (1.0)	–

Table 2. Mean (SD) estimated fracture load, and unadjusted and BW-adjusted mean percentage differences (95% CI) in the fracture load between the exercise loading group and the control group.

Group	Mean (SD) in N	Unadjusted		Weight-adjusted	
		% diff	*p*	% diff	*p*
H-I	3228 (408)	14.6 (6.2 to 23.6)	**0.014**	14.3 (6.7 to 22.5)	**0.008**
O-I	3164 (447)	12.0 (3.5 to 21.3)	**0.045**	11.4 (3.2 to 20.3)	**0.049**
H-M	2960 (584)	3.9 (-5.6 to 14.4)	0.553	0.2 (-7.5 to 8.8)	0.948
R-I	3231 (538)	14.0 (4.4 to 24.4)	**0.034**	26.2 (16.2 to 36.9)	**<0.001**
R-NI	3068 (500)	8.3 (-0.5 to 18.0)	0.177	2.1 (-6.0 to 10.6)	0.741
Control	2849 (551)	-	-	-	-

Statistically significant *p* values ($p < 0.05$) based on ANOVA and ANCOVA are shown in bold.

Table 3. Mean (SD) and ranges of the fracture location in the *polar angle* and the *relative axial location,* and *p*-values for the difference between the exercise loading group and the control group.

	Polar angle (°)			Relative axial location (%)		
Group	Mean (SD)	Range	*p*	Mean (SD)	Range	*p*
H-I	30.1 (14.0)	13.3° to 59.5°	0.214	90.1 (16.9)	65.6% to 130.0%	**0.038**
O-I	30.7 (15.3)	10.9° to 74.8°	0.224	86.8 (9.9)	50% to 96.2%	**<0.001**
H-M	41.0 (24.0)	14.8° to 86.4°	0.821	97.0 (5.5)	85.7% to 104.5%	0.798
R-I	36.5 (19.8)	7.0° to 81.4°	0.828	98.0 (10.8)	77.8% to 119.0%	0.919
R-NI	35.4 (13.0)	17.7° to 68.5°	0.965	92.7 (14.2)	69.2% to 116.7%	0.317
Control	35.6 (13.7)	15.6° to 72.3°	-	97.0 (8.3)	84.0% to 122.7%	-

Statistically significant *p* values ($p < 0.05$) based on Mann-Whitney U tests are shown in bold.

Table 4: Anatomical regional fracture location in different groups

Group	N	*Polar angular location*			*Relative axial location*			
		Superior	Supero-posterior	Posterior	Cervical			Trochanteric
					Sub-capital	Trans-cervical	Basi-cervical	
H-I	19	6	13	0	0	1	15	3
O-I	19	6	12	1	0	1	18	0
H-M	17	4	9	4	0	0	14	3
R-I	18	4	12	2	0	0	13	5
R-NI	18	4	13	1	0	0	13	5
Control	20	3	16	1	0	0	17	3